Monitoring kidney optical properties during cold storage preservation with spatial frequency domain imaging

Rebecca Rowland
Adrien Ponticorvo
Alberto Jarrin Lopez
Shiri Li
Xiaodong Li
Hirohito Ichii
Anthony J. Durkin

SPIE.

Monitoring kidney optical properties during cold storage preservation with spatial frequency domain imaging

Rebecca Rowland,[a] Adrien Ponticorvo,[a] Alberto Jarrin Lopez,[b] Shiri Li,[b] Xiaodong Li,[c] Hirohito Ichii,[b] and Anthony J. Durkin[a,d,*]
[a]University of California, Irvine, Beckman Laser Institute and Medical Clinic, Irvine, California, United States
[b]University of California, Irvine, Department of Surgery, UC Irvine Division of Transplantation, Orange, California, United States
[c]UC Irvine Health Douglas Hospital, Department of Pathology, Orange, California, United States
[d]University of California, Irvine, Department of Biomedical Engineering, Irvine, California, United States

Abstract. Transplantation of kidneys results in delayed graft function in as many as 40% of cases. During the organ transplantation process, donor kidneys undergo a period of cold ischemic time (CIT), where the organ is preserved with a cold storage solution to maintain tissue viability. Some complications observed after grafting may be due to damage sustained to the kidney during CIT. However, the effects due to this damage are not apparent until well after transplant surgery has concluded. To this end, we have used spatial frequency domain imaging (SFDI) to measure spatially resolved optical properties of porcine kidneys over the course of 80-h CIT. During this time, we observed an increase in both reduced scattering (μ_s') and absorption (μ_a) coefficients. The measured scattering b parameter increased until 24 h of CIT, then returned toward baseline during the remaining duration of the imaging sequence. These results show that the optical properties of kidney tissue change with increasing CIT and suggest that continued investigation into the application of SFDI to kidneys under CIT may lead to the development of a noninvasive method for assessing graft viability. © *The Authors. Published by SPIE under a Creative Commons Attribution 4.0 Unported License. Distribution or reproduction of this work in whole or in part requires full attribution of the original publication, including its DOI.* [DOI: 10.1117/1.JBO.24.11.116003]

Keywords: spatial frequency domain imaging; organ transplantation; kidney, cold storage preservation; tissue optics.

Paper 190284RR received Aug. 26, 2019; accepted for publication Nov. 11, 2019; published online Nov. 27, 2019.

1 Introduction

Renal failure, due to complications such as glomerular disease, diabetes, vascular disease, or hypertension, often necessitates a kidney transplant. In the United States, the number of kidney transplantations makes up the majority of organ transplantation procedures at around 21,000 annually.[1] Currently, 74,000 patients are active on the waitlist, 113,000 patients are on the total waitlist, and the number of patients has been increasing by about 8% every year.[1] About 32% of patients receive transplants from living donors, but the remaining 68% receive kidneys from deceased donors.[2] To facilitate this operation, kidneys from the deceased donor are generally preserved in a cold storage solution during a period called cold ischemic time (CIT).[3,4] During the CIT, preserved kidneys are kept at a temperature of 4°C, to decrease the metabolic rate and thereby maintain tissue viability given the lower oxidative damage.[5] However, kidney preservation results in renal ischemia and the subsequent generation of reactive oxygen species due to anaerobic glycolysis.[6,7] This can cause acute tubular necrosis leading to delayed graft function. It is estimated that as many as 40% of deceased donor kidneys undergo some kind of delayed graft function.[8] As a result, patients must undergo dialysis therapy after transplantation, which increases risk for acute rejection of the grafted kidney.[9] However, it is difficult to predict if the patient will experience delayed graft function until after transplantation. Explicit criteria for discarding potential donor kidneys are not standardized, which has led to high discard rates within the United States.[10] In 2015, almost one-fifth of procured kidneys were discarded.[11] The discard rate is higher (42%) in cases of marginal donors, who have increased risk factors such as advanced age, hypertension, or diabetes.[12] Evaluation of pretransplant biopsies is time consuming, subject to variable assessment, and is performed in fewer than 20% of standard donor cases and fewer than 80% of marginal donor cases.[13] Determining the quality of kidney pretransplant has become increasingly important, as the demand for kidney transplants rises and centers move toward accepting more kidneys from marginal donors.[14]

Optical imaging techniques have been used in animal models and clinical research to monitor ischemia/reperfusion injury in kidneys during the postreperfusion period and to aid clinicians in pinpointing circumstances of delayed graft function. Fluorescence imaging with indocyanine green (ICG) has been performed intraoperatively to assess the condition of reconstructed arteries and veins after tissue grafting.[15–20] Laser Doppler flowmetry (LDF) has provided a means for measuring renal blood flow after reperfusion.[21–28] Tissue oxygenation in grafted kidneys has been measured using near-infrared spectroscopy (NIRS).[15,29–31] Optical coherence tomography (OCT) has been used to assess structural changes to proximal convoluted tubules and glomeruli.[32–36] Multiphoton microscopy has been used in rodent studies to probe a number of fluorescent markers for structural and functional changes in kidneys at micron-level resolution.[37–42] During studies that involve human patients, imaging is performed after grafting and reperfusion of the kidney. In experiments with small animal models, the blood flow into the kidneys is stopped through clamping of the renal artery and

*Address all correspondence to Anthony J. Durkin, E-mail: aadurin@uci.edu

then reintroduced during the course of imaging. These studies focus on the reperfusion period, after the transplantation has already been performed. While this has led to a better evaluation of the effects of warm ischemic time during procedures such as partial nephrectomy, the methodology used in the majority of these studies is not fully analogous to what kidneys undergo during harvest and preservation for transplantation. Little has been reported on the optical properties of kidneys during preservation under CIT conditions or before reperfusion of the graft.

Here, we used spatial frequency domain imaging (SFDI) to characterize the optical changes that occur in kidneys during the period of cold ischemia. SFDI is a noninvasive, wide-field optical imaging technique that can be used to quantify spatially resolved, wavelength-dependent absorption, and reduced scattering coefficients at multiple wavelengths using structured illumination. The absorption coefficient can be further distilled using Beer's law and a linear least squares fit to determine the oxy- and deoxyhemoglobin concentrations.[43,44] The reduced scattering coefficient provides insight into subsurface tissue structure.[45] Previously, we have used SFDI to monitor *in-vivo* porcine kidney during the period of renal arterial occlusion,[46] in a manner similar to procedures that have employed OCT, NIRS, LDF, and ICG in animal studies. In this paper, we instead use SFDI to track the optical properties of freshly excised porcine kidneys that have been handled under typical cold storage conditions, including immersion in University of Wisconsin cold storage solution (UW solution).[47,48] Measurements using SFDI are reported periodically to monitor changes in optical properties as the length of CIT increased. A more complete understanding of the structural changes in kidneys during CIT may provide new insights regarding the overall health and viability of kidney tissue before surgery and reperfusion.

2 Methodology

2.1 Cold Storage Preservation

In total, six kidneys, three left and three right, were harvested with care from three Yorkshire pigs. Kidneys were removed postmortem and perfused with UW solution through the renal artery. Perfused kidneys were immersed in UW solution and stored over ice in between imaging sessions, according to typical preservation protocol as indicated by our clinical colleague. Ideally, kidneys can be safely stored in UW solution for a maximum of 72 h.[48] In practice, typical mean CIT is closer to 24 h,[47,49] and the more realistic maximum CIT is near 40 h.[49] Here, the kidneys were preserved and periodically imaged for 80 h, to capture changes in optical properties that might occur within the maximum usage timeframe associated with viable kidneys.

2.2 Histology

For one of the three pigs used, we took 4-mm-diameter biopsies from the right kidney. Biopsies were taken along the kidney renal cortex at 30 min, 24 h, and 80 h postharvest. Samples were fixed for 24 h in 10% neutral buffered formalin, dehydrated with alcohol, prepared in the xylazine alternative histoclear, and embedded in paraffin wax. Sections of 2 μm size were stained with periodic acid-Schiff (PAS).

2.3 Spatial Frequency Domain Imaging

SFDI is a noninvasive imaging technique that measures optical properties over a wide field of view by projecting sinusoidally patterned illumination at multiple wavelengths and spatial frequencies.[50,51] We employed the OxImager RS® (Modulim, Inc., Irvine, California), a commercial SFDI device. This instrument measures tissue reflectance at eight wavelengths (471, 526, 591, 621, 659, 691, 731, and 851 nm) and five spatial frequencies (0, 0.05, 0.10, 0.15, and 0.20 mm^{-1}) over a large field of view (20×15 cm).[50] The ventral side of each kidney was imaged at 0.5, 1.5, 21, 24, 29, 45, 53, 70, and 80 h after harvest and reperfusion with UW solution. After measuring the kidneys with SFDI, they were returned to a container of UW solution. Kidneys were not removed from UW solution for more than 3 min at a time for imaging.

Raw SFDI reflectance maps at all eight wavelengths and spatial frequencies were demodulated, corrected for height (± 20 mm) and angle (± 30 deg) variation, and calibrated against a silicone tissue-simulating phantom with known optical properties.[52] Optical property maps for the absorption and reduced scattering coefficients were rendered using the look-up table method that we have described in detail previously.[43] The scattering b parameter for measured tissue was calculated by fitting the reduced scattering values measured for wavelengths (λ) 659, 731, and 851 nm to a power law function:

$$\mu_s' = A\left(\frac{\lambda}{\lambda_0}\right)^{-b},$$

where $\lambda_0 = 800$ nm.

This function, derived from Mie theory, has been used in the near-infrared regime to relate scattering slope to the size of the scattering particles.[53,54] At these longer wavelengths, the contribution to the scattering slope b can be better estimated by Mie scattering, and less so by Rayleigh.[45,53,55]

Further image processing of optical property maps was performed using MATLAB R2018a (MathWorks, Natick, Massachusetts). After rendering optical property maps of each kidney, regions of interest (ROIs) were selected from the renal cortex within the upper pole of each kidney, which contains the filtering nephrons essential to kidney function.[56] These ROIs were selected so as to avoid measurement artifacts due to specular reflection from the kidney surface.

The OxImager RS® was also used to record color photography of each kidney at each imaging time point, under controlled lighting conditions. The red color channel was extracted from these images in order to illustrate in a semiquantitative way, and Fig. 1 shows the visible color changes (or lack thereof) in the tissue over time. This examination of the appearance of the kidneys during CIT resembles what the clinician would observe before transplantation.

3 Results

3.1 Clinical Appearance, Color, and Histology

The color (RGB) of each kidney appeared to change very little over the 80 h of periodic documentation. Color photographs (RGB) taken of the left kidney of the third pig are depicted in row 1 of Fig. 1(a). Maps of the red color channel of the left kidney of the third pig are shown in row 2 of Fig. 1(a).
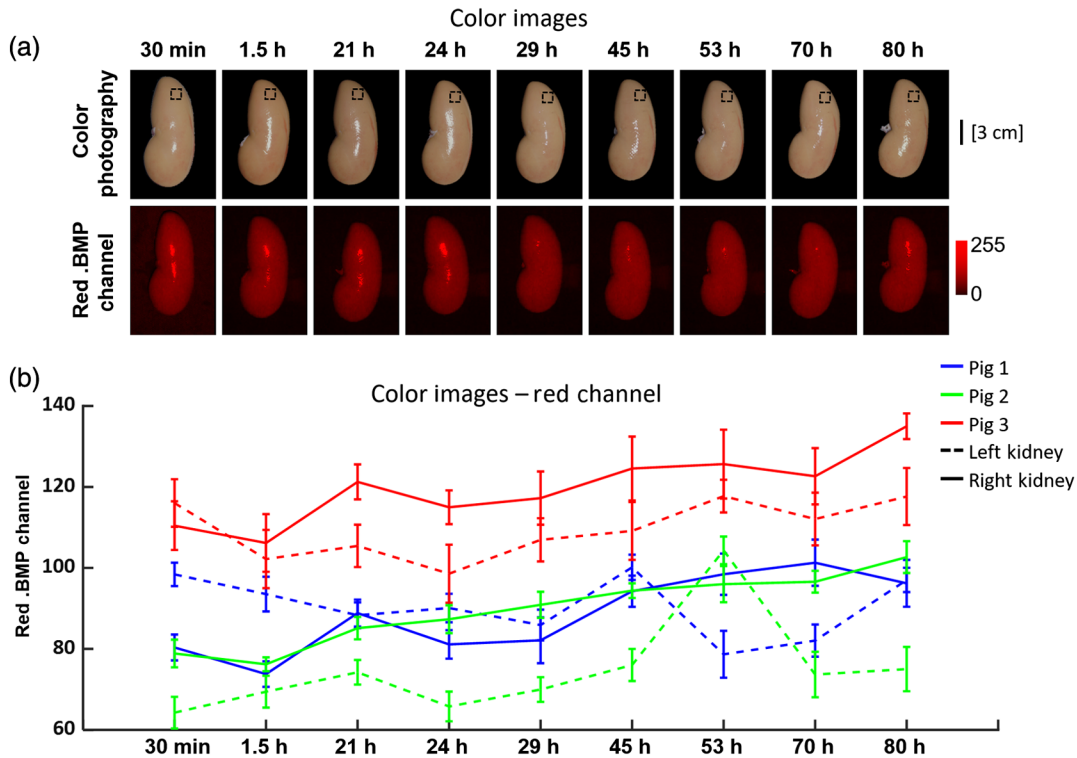
Fig. 1 Typical example of kidney appearance over time. (a) Color images (RGB) of kidney and red channel images from corresponding.bmp map from the left kidney of the third pig. (b) Graph of all red channel values at measured post-UW perfusion time points for all kidneys.

On average, the value of the red color channel increased by 14.8% by 80-h post-UW perfusion.

PAS-stained slides were read for tissue sections taken from biopsy samples corresponding to imaging time points of 30 min, 24 h, and 80 h of cold storage. Typical histology is presented in Fig. 2. After 30 min under CIT, the histology indicated sparse apical blebing and little damage to the brush borders (arrows, Fig. 2). After 24 h, more brush border damage was apparent. By 80 h, early infiltration of inflammatory cells was observed

(circled region, Fig. 2), in addition to the brush border damage (arrows). However, these changes were relatively acute and not present throughout the entire volume of the biopsy sample.

3.2 Reduced Scattering Coefficient

From the eight wavelengths used by the SFDI device, the 659-nm wavelength showed the most change over the time course of imaging, shown as percent increase in Table 1. Values of the
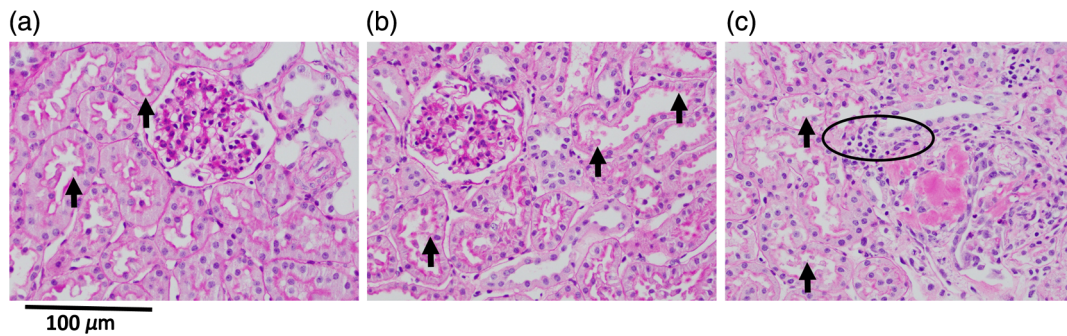

Fig. 2 PAS-stained biopsies from (a) 30-min, (b) 24-h, and (c) 80-h postprocurement. Arrows indicate brush border damage. Areas of inflammation are circled.

Table 1 Average percent increase in reduced scattering coefficient from 30 min to 80 h of CIT for eight wavelengths.

Wavelength (nm)	471	526	591	621	659	691	731	851
μ_s' Increase from 30-min to 80-h CIT (%)	30.3	34.5	34.8	34.3	50.4	33.9	33.9	34.4

reduced scattering coefficient measured at 659 nm over 80 h are shown in Fig. 3(a). On average, the reduced scattering coefficient increased by 50.4% by 80-h post-UW perfusion. Maps of the reduced scattering values measured at 659 nm of the left kidney from the third pig are shown in Fig. 3(b).

3.3 Scattering b Parameter

Values of the scattering *b* parameter measured over 80 h are shown in Fig. 4(a). On average, the *b* parameter increased by 58.77% by 24-h post-UW perfusion. After the 24-h time point, the *b* parameter returned toward the initial values, and at 80-h postperfusion, it was only 1.01% above 30-min postperfusion measurement. Maps of the *b* parameter measured on the left kidney from the third pig are shown in Fig. 4(b).

3.4 Absorption Coefficient

Values of the absorption coefficient measured with 659 nm over 80 h are shown in Fig. 5(a). On average, the absorption coefficient increased by 23.4% within 21-h post-UW perfusion and 31.4% by 80 h. Maps of the absorption values of the left kidney from the third pig measured at 659 nm are shown in Fig. 5(b).

4 Discussion

There was little change observed in appearance of the kidneys over the course of experiment, either in the corresponding color photographs or in the more quantitative analysis of the individual RGB red channel. This highlights the challenge posed to transplantation specialists, who currently cannot visually assess underlying structural changes accrued during CIT.
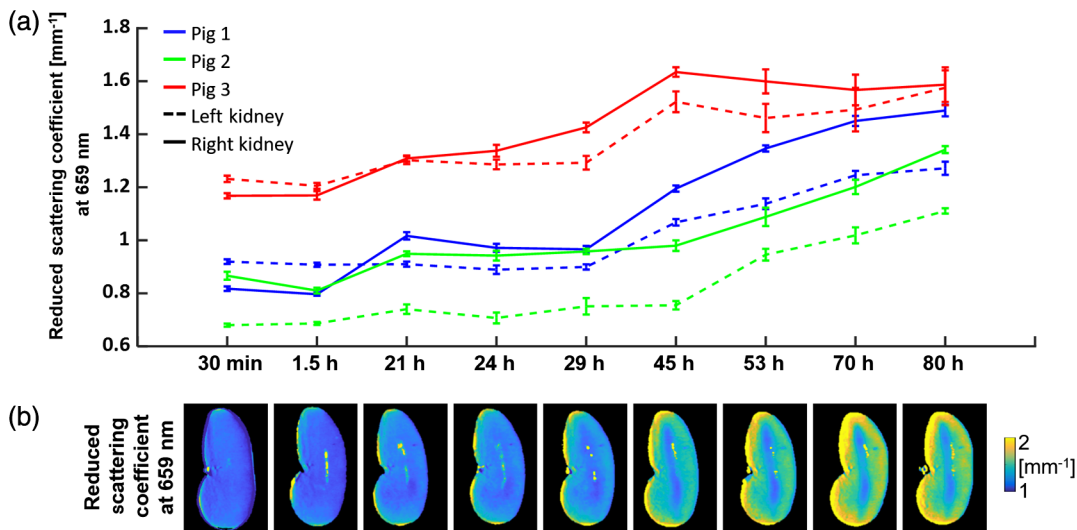

Fig. 3 Time dependence of change in reduced scattering coefficient. (a) Graph of reduced scattering coefficient values measured at 659 nm for all kidneys at nine time points post-UW perfusion. (b) Spatially resolved maps of reduced scattering coefficient of the left kidney from pig 3, measured at 659 nm.
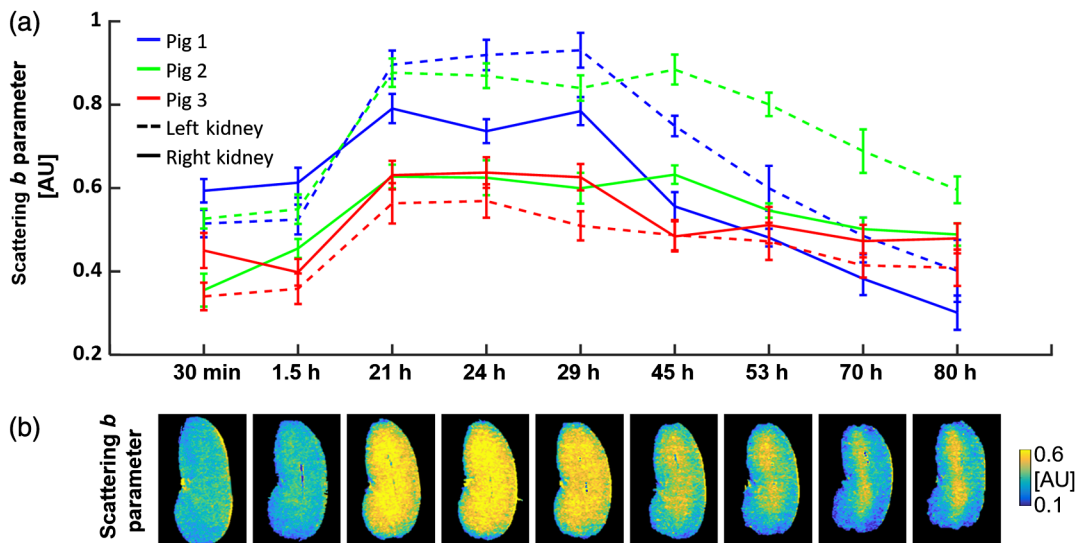

Fig. 4 Time dependence of change in *b* parameter. (a) Graph of scattering *b* parameter measured at nine time points post-UW perfusion. (b) Scattering *b* parameter maps of the left kidney from pig 3.
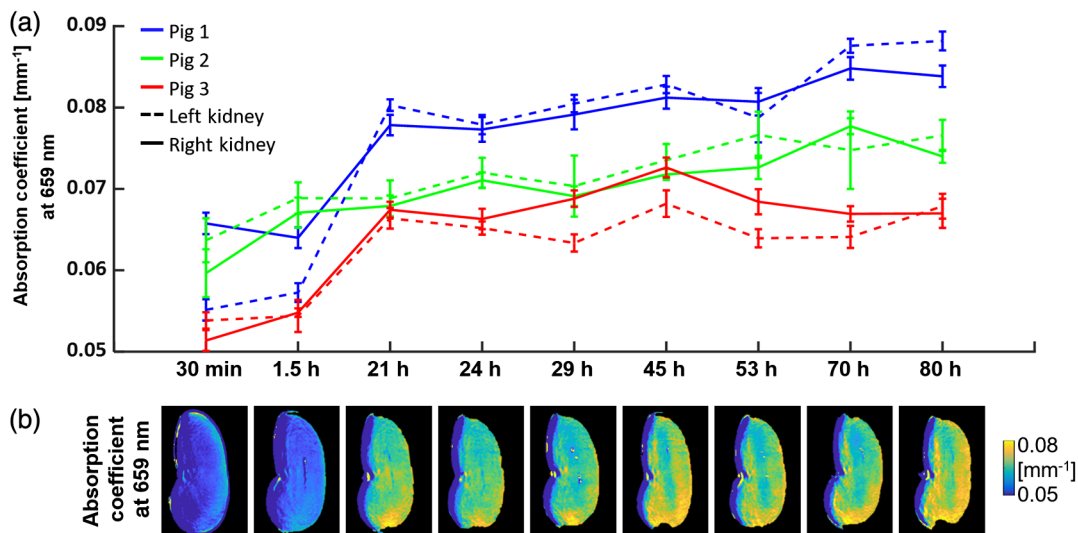
Fig. 5 Time dependence of change in absorption coefficient. (a) Graph of absorption coefficient at 659 nm measured at nine time points post-UW perfusion. (b) Maps of absorption coefficient measured at 659 nm of the left kidney from pig 3.

Previous studies on kidney transplantation in animal models using ICG, LDF, NIRS, and SFDI imaging techniques simulated the ischemia/reperfusion injury through *in-vivo* renal arterial occlusion. In this study, kidneys are measured *ex vivo* while the kidney is preserved in UW cold storage solution. The absorption measurements made here with SFDI do not relate to any hemodynamic changes, as blood is flushed from each kidney using UW solution. Still, absorption measured with 659-nm light indicated a 23.4% increase between 30-min and 21-h post-UW perfusion. The absorption continued to gradually increase during the remaining time course of this study while the kidney was still preserved with UW solution.

A preceding SFDI study measured *in-vivo*, blood perfused porcine kidneys during an 80-min renal arterial occlusion using an occlusion balloon cuff.[46] The reduced scattering coefficient (μ_s') was measured at 658, 732, and 850 nm, and increased during the occlusion period (1 h totally) but held steady between 4 and 52 min of occlusion. The reduced scattering coefficient returned to baseline after release of the occlusion cuff. The *b* parameter decreased during this period of occlusion from 1.05 to 0.88. This change in μ_s' and *b* was attributed to the edema increase resulting from the inflammatory response.

The measurements detailed in the experiment presented here also show an increase in reduced scattering during the period of ischemia. This increase lasts throughout the duration of the 80-h time period, indicating continuous structural change within the kidneys during CIT. Changes in the values for the *b* parameter during the first 1.5 h differ from kidney to kidney, unlike in the previous SFDI ischemia-reperfusion study, but this may be due to differences in the method of ischemia. In this previous study, the kidneys were occluded but not cleared of blood, and changes in absorption were only reported through measurements of oxygen saturation. The kidneys in our study were removed from the animal, cleared of blood via perfusion with UW solution, and then stored in UW solution so no direct comparison between absorption and oxygen saturation could be made. Additionally, changes observed within the first few hours of cold ischemia are minimal compared to the changes in *b* seen after a day of storage in UW. At 24-h post-UW perfusion, the *b* parameter reaches a peak value, with an average increase of 58.77% from the first measurement. During ischemia, the kidney can no longer undergo aerobic respiration and must create ATP through glycolysis.[6] This in turn causes a buildup in potassium and sodium ions across cell membranes. In this case, the ion imbalance results in cell swelling, which would affect the μ_s' and *b* parameter. However, no cell volume change was observed within the histology, suggesting that the change in scattering may only be due to an uptick in inflammatory mediators.[6] After 24 h of CIT, the *b* parameter begins to decrease. Finally, values of *b* recover to near baseline by the end of the 80-h period, which is past the maximum 72-h time point recommended for kidney transplant viability after CIT. This observation raises the question of how the *b* parameter, which is closely related to scattering particle size, may seemingly recuperate. An understanding of the change in *b* after 24 h of CIT would likely require analysis of the anisotropy ratio (*g*), a component of the reduced scattering coefficient that changes with wavelength and tissue structure.[57] Additionally, while the changes seen in PAS-stained slides marked brush border damage and inflammation at later time points seemed to correspond with increasing scattering, as was observed in the previous SFDI study, the histopathology also suggested that these changes were acute.[46] Further investigation into the effects of CIT on kidney optical properties with SFDI would also benefit from varying the length of ischemic time between kidney harvest and perfusion with UW solution.

5 Conclusion

In this investigation, SFDI-derived reduced scattering and scattering *b* parameter suggest the occurrence of structural changes within excised kidneys during the period of CIT. Further investigation of this change in scattering and *b* parameter, especially at additional time points between kidney removal and 24-h post-UW perfusion, may lead to a better understanding of structural injury that occurs during initial kidney removal and CIT. A detailed comparison of kidneys that undergo different durations of ischemia before being cleared with UW may also enable a better understanding of how SFDI, particularly the measured

scattering parameters, can be used to noninvasively screen for damaged kidney grafts before transplantation and reperfusion in a patient.

References

1. United Network for Organ Sharing, "Transplant trends," 2019, https://unos.org/data/transplant-trends/.
2. U.S. Department of Health and Human Services, "Organ procurement and transplant network national data," 2019, https://optn.transplant.hrsa.gov/data/view-data-reports/national-data/#.
3. G. R. Hetzel et al., "Risk factors for delayed graft function after renal transplantation and their significance for long-term clinical outcome," *Transplant Int.* **15**(1), 10–16 (2002).
4. T. W. L. Scheeren et al., "Prognostic value of intraoperative renal tissue oxygenation measurement on early renal transplant function," *Transplant Int.* **24**(7), 687–696 (2011).
5. M. D. Kay et al., "Comparison of preservation solutions in an experimental model of organ cooling in kidney transplantation," *Br. J. Surg.* **96**(10), 1215–1221 (2009).
6. C. E. Ponticelli, "The impact of cold ischemia time on renal transplant outcome," *Kidney Int.* **87**(2), 272–275 (2015).
7. A. Debout et al., "Each additional hour of cold ischemia time significantly increases the risk of graft failure and mortality following renal transplantation," *Kidney Int.* **87**(2), 343–349 (2015).
8. P. M. Buchanan et al., "The clinical and financial burden of early dialysis after deceased donor kidney transplantation," *J. Nephrol. Ther.* **S4**, 001 (2011).
9. A. Siedlecki, W. Irish, and D. C. Brennan, "Delayed graft function in the kidney transplant," *Am. J. Transplant.* **11**(11), 2279–2296 (2011).
10. S. Mohan et al., "The weekend effect alters the procurement and discard rates of deceased donor kidneys in the United States," *Kidney Int.* **90**(1), 157–163 (2016).
11. D. E. Stewart et al., "Diagnosing the decades-long rise in the deceased donor kidney discard rate in the United States," *Transplantation* **101**(3), 575–587 (2017).
12. B. Tanriover et al., "Kidneys at higher risk of discard: expanding the role of dual kidney transplantation," *Am. J. Transplant.* **14**(2), 404–415 (2014).
13. R. S. Sung et al., "Determinants of discard of expanded criteria donor kidneys: impact of biopsy and machine perfusion," *Am. J. Transplant.* **8**(4), 783–792 (2008).
14. J. Treckmann et al., "Machine perfusion versus cold storage for preservation of kidneys from expanded criteria donors after brain death," *Transplant Int.* **24**(6), 548–554 (2011).
15. W. Polom et al., "Usage of invisible near infrared light (NIR) fluorescence with indocyanine green (ICG) and methylene blue (MB) in urological oncology. Part 1," *Cent. Eur. J. Urol.* **67**(2), 142–148 (2014).
16. M. Sekijima et al., "An intraoperative fluorescent imaging system in organ transplantation," *Transplant Proc.* **36**(7), 2188–2190 (2004).
17. N. Arichi et al., "Intraoperative fluorescence vascular imaging using indocyanine green for assessment of transplanted kidney perfusion," *Transplant Proc.* **46**(2), 342–345 (2014).
18. C. Hoffmann et al., "Intraoperative assessment of kidney allograft perfusion by laser-assisted indocyanine green fluorescence videography," *Transplant Proc.* **42**(5), 1526–1530 (2010).
19. U. Rother et al., "Dosing of indocyanine green for intraoperative laser fluorescence angiography in kidney transplantation," *Microcirculation* **24**(8) (2017).
20. T. Sawada et al., "An alternative tool for intraoperative assessment of renal vasculature after revascularization of a transplanted kidney," *Am. J. Surg.* **199**(6), e69–e71 (2010).
21. L. Gaschen and H. J. Schuurman, "Ultrasound score is more predictive than serum creatinine in assessment of cellular rejection in cynomolgus monkey renal allografts," *Invest. Radiol.* **37**(7), 376–380 (2002).
22. F. T. Hammad et al., "Intra- and post-operative assessment of renal cortical perfusion by laser Doppler flowmetry in renal transplantation in the rat," *Eur. Surg. Res.* **32**(5), 284–288 (2000).
23. M. Luger-Hamer et al., "Renal viability evaluated by the multiprobe assembly: a unique tool for the assessment of renal ischemic injury," *Nephron Clin. Pract.* **111**(1), c29–c38 (2009).
24. C. McArthur, C. C. Geddes, and G. M. Baxter, "Early measurement of pulsatility and resistive indexes: correlation with long-term renal transplant function," *Radiology* **259**(1), 278–285 (2011).
25. G. Mocny et al., "The value of Doppler ultrasound in predicting delayed graft function occurrence after kidney transplantation," *Folia Med. Cracov.* **56**(4), 51–62 (2016).
26. M. Naef et al., "Evaluation of laser Doppler flowmetry to assess cyclosporine A-induced impairment of renal blood flow," *J. Surg. Res.* **75**(2), 161–164 (1998).
27. S. Takahashi et al., "Acute renal allograft rejection in the canine: evaluation with serial duplex Doppler ultrasonography," *Transplant Proc.* **31**(3), 1731–1734 (1999).
28. T. Yanagisawa et al., "Evaluation of laser Doppler flowmetry in renal transplantation," *J. Clin. Laser Med. Surg.* **12**(4), 231–232 (1994).
29. G. Malakasioti et al., "Continuous monitoring of kidney transplant perfusion with near-infrared spectroscopy," *Nephrol. Dial. Transplant.* **33**(10), 1863–1869 (2018).
30. E. Vidal et al., "Near-infrared spectroscopy as continuous real-time monitoring for kidney graft perfusion," *Pediatr. Nephrol.* **29**(5), 909–914 (2014).
31. T. Gladytz et al., "Near infrared spectroscopy system for quantitative monitoring of renal hemodynamics and oxygenation in rats," *Proc. SPIE* **10874**, 108740H (2019).
32. P. M. Andrews et al., "Optical coherence tomography of the aging kidney," *Exp. Clin. Transplant.* **14**(6), 617–622 (2016).
33. P. M. Andrews et al., "Optical coherence tomography of the living human kidney," *J. Innov. Opt. Health Sci.* **7**(2), 1350064 (2014).
34. Y. Chen et al., "High-resolution three-dimensional optical coherence tomography imaging of kidney microanatomy *ex vivo*," *J. Biomed. Opt.* **12**(3), 034008 (2007).
35. M. Gupta and L. M. Su, "Current and evolving uses of optical coherence tomography in the genitourinary tract," *Curr. Urol. Rep.* **16**(3), 15 (2015).
36. Z. F. Li et al., "Monitoring kidney microanatomy changes during ischemia-reperfusion process using texture analysis of OCT images," *IEEE Photonics J.* **9**(2), 4000110 (2017).
37. A. M. Hall et al., "Multiphoton imaging of the functioning kidney," *J. Am. Soc. Nephrol.* **22**(7), 1297–1304 (2011).
38. A. M. Hall et al., "*In vivo* multiphoton imaging of mitochondrial structure and function during acute kidney injury," *Kidney Int.* **83**(1), 72–83 (2013).

39. S. L. Ashworth et al., "Two-photon microscopy: visualization of kidney dynamics," *Kidney Int.* **72**(4), 416–421 (2007).
40. M. Horbelt et al., "Acute and chronic microvascular alterations in a mouse model of ischemic acute kidney injury," *Am. J. Physiol. Renal Physiol.* **293**(3), F688–F695 (2007).
41. T. A. Sutton et al., "Injury of the renal microvascular endothelium alters barrier function after ischemia," *Am. J. Physiol. Renal Physiol.* **285**(2), F191–F198 (2003).
42. G. Camirand et al., "Multiphoton intravital microscopy of the transplanted mouse kidney," *Am. J. Transplant.* **11**(10), 2067–2074 (2011).
43. D. J. Cuccia et al., "Quantitation and mapping of tissue optical properties using modulated imaging," *J. Biomed. Opt.* **14**(2), 024012 (2009).
44. D. J. Cuccia et al., "Quantitative *in vivo* imaging of tissue absorption, scattering, and hemoglobin concentration in rat cortex using spatially modulated structured light," in *In Vivo Optical Imaging of Brain Function*, 2nd ed., R. D. Frostig, Ed., CRC Press/Taylor & Francis, Boca Raton, Florida (2009).
45. S. L. Jacques, "Optical properties of biological tissues: a review," *Phys. Med. Biol.* **58**(11), R37–R61 (2013).
46. K. P. Nadeau et al., "Quantitative assessment of renal arterial occlusion in a porcine model using spatial frequency domain imaging," *Opt. Lett.* **38**(18), 3566–3569 (2013).
47. J. H. Southard and F. O. Belzer, "Organ preservation," *Annu. Rev. Med.* **46**, 235–247 (1995).
48. F. Muhlbacher, F. Langer, and C. Mittermayer, "Preservation solutions for transplantation," *Transplant Proc.* **31**(5), 2069–2070 (1999).
49. R. J. Ploeg et al., "Effect of preservation solution on results of cadaveric kidney-transplantation," *Lancet* **340**(8812), 129–137 (1992).
50. D. J. Cuccia et al., "Modulated imaging: quantitative analysis and tomography of turbid media in the spatial-frequency domain," *Opt. Lett.* **30**(11), 1354–1356 (2005).
51. D. J. Cuccia, "Spatial frequency domain imaging (SFDI): a technology overview and validation of an LED-based clinic-friendly device," *Proc. SPIE* **8254**, 825405 (2012).
52. G. M. Palmer and N. Ramanujam, "Monte Carlo-based inverse model for calculating tissue optical properties. Part I: theory and validation on synthetic phantoms," *Appl. Opt.* **45**(5), 1062–1071 (2006).
53. X. Wang et al., "Approximation of Mie scattering parameters in near-infrared tomography of normal breast tissue *in vivo*," *J. Biomed. Opt.* **10**(5), 051704 (2005).
54. F. Bevilacqua et al., "Broadband absorption spectroscopy in turbid media by combined frequency-domain and steady-state methods," *Appl. Opt.* **39**(34), 6498–6507 (2000).
55. H. Jonasson et al., "*In vivo* characterization of light scattering properties of human skin in the 475- to 850-nm wavelength range in a Swedish cohort," *J. Biomed. Opt.* **23**(12), 121608 (2018).
56. B. Kaissling and M. Le Hir, "The renal cortical interstitium: morphological and functional aspects," *Histochem. Cell Biol.* **130**(2), 247–262 (2008).
57. R. Samatham and S. L. Jacques, "Determine scattering coefficient and anisotropy of scattering of tissue phantoms using reflectance-mode confocal microscopy," *Proc. SPIE* **7187**, 718711 (2009).

Biographies of the authors are not available.